Accelerating Hydrogen Evolution at Neutral pH by Destabilization Water with Conducting Oxophilic Metal Oxide

Zhengzhe Xie,[ab†] Wugang Wang,[c†] Ding Ding,[d] Yu Zou,[*ab] Yi Cui,[d] Lai Xu[*c] and Jiang Jiang[*ab]

[a]School of Nano-Tech and Nano-Bionics, University of Science and Technology of China, Hefei 230026, China

[b]i-Lab, CAS Key Laboratory of Nano-Bio Interface, CAS Center for Excellence in Nanoscience, Suzhou Institute of Nano-Tech and Nano-Bionics, Chinese Academy of Sciences, Suzhou 215123, China.

[c]Institute of Functional Nano & Soft Materials (FUNSOM), Jiangsu Key Laboratory for Carbon-Based Functional Materials & Devices, Soochow University, 199 Ren'ai Road, Suzhou 215123, China

[d]Vacuum Interconnected Nanotech Workstation, Suzhou Institute of Nano-Tech and Nano-Bionics, Chinese Academy of Sciences, Suzhou 215123, China

†These authors contributed equally to this work.

Supplementary information

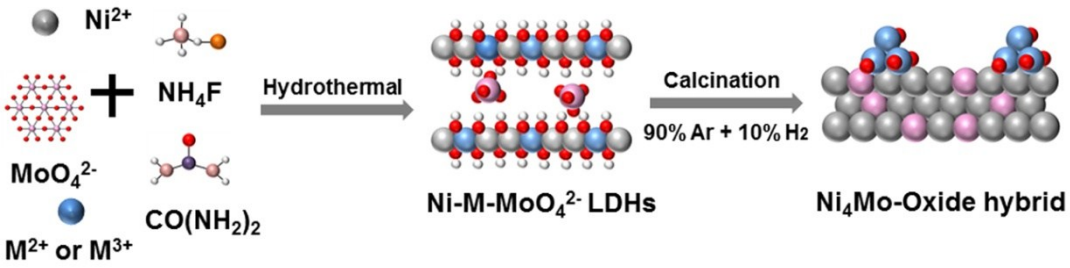

Fig. S1 Schematic illustration of the synthetic procedures of producing various Ni_4Mo-metal oxides hybrids by topotactic transformation of MoO_4^{2-} intercatalated Ni-M-LDH (M = Zn, Mn, Cr, V).

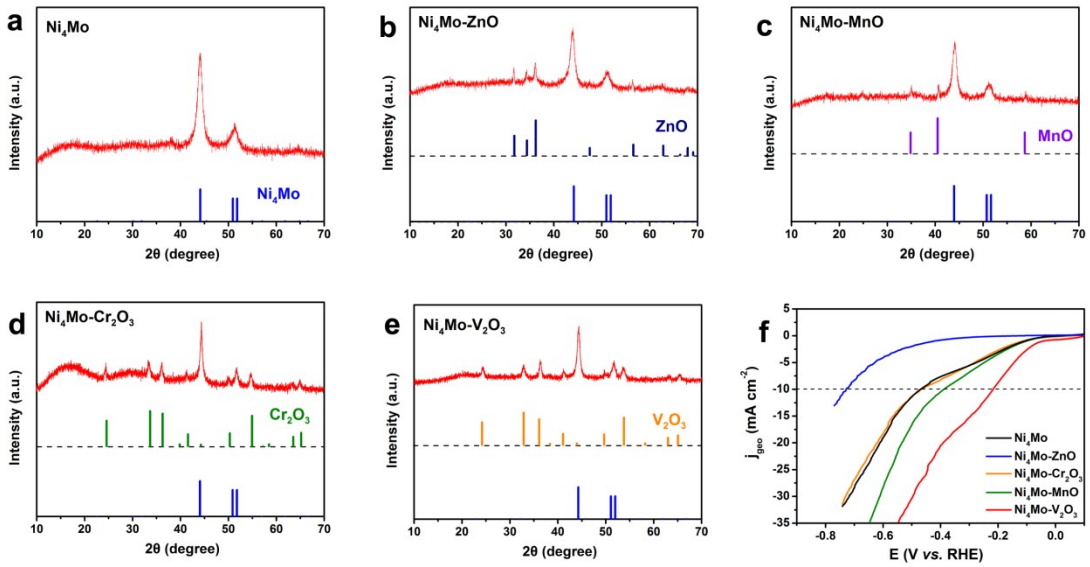

Fig. S2 XRD patterns of (a) Ni_4Mo (Ni_4Mo: JCPDS No.03-1036), (b) Ni_4Mo-ZnO (ZnO: JCPDS No.36-1451), (c) Ni_4Mo-MnO (MnO: JCPDS No.07-0230), (d) Ni_4Mo-Cr_2O_3 (Cr_2O_3: JCPDS No.38-1479) and (e) Ni_4Mo-V_2O_3 (V_2O_3: JCPDS No.34-0187), (f) Polarization curves of Ni_4Mo and Ni_4Mo-metal oxide (Ni_4Mo-ZnO, Ni_4Mo-MnO, Ni_4Mo-Cr_2O_3, Ni_4Mo-V_2O_3) on GCE in 1 M PBS.

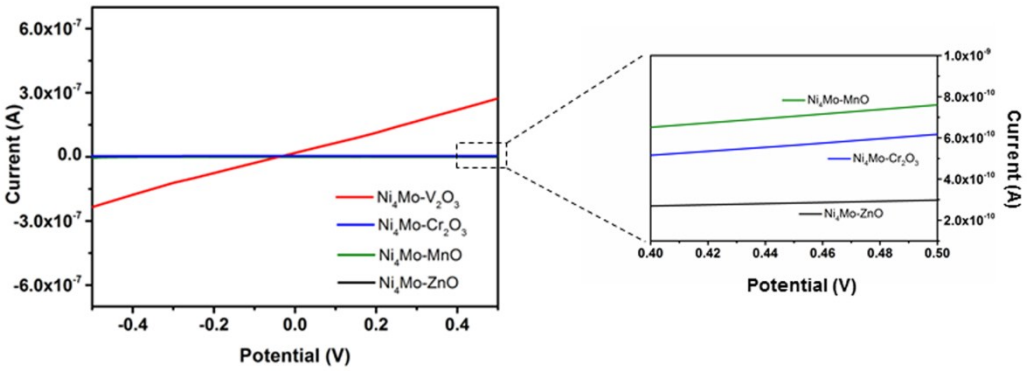

Fig. S3 I-V curves of Ni_4Mo-V_2O_3, Ni_4Mo-Cr_2O_3, Ni_4Mo-MnO, and Ni_4Mo-ZnO powders, showing magnitude higher electron conductivity of Ni_4Mo-V_2O_3.

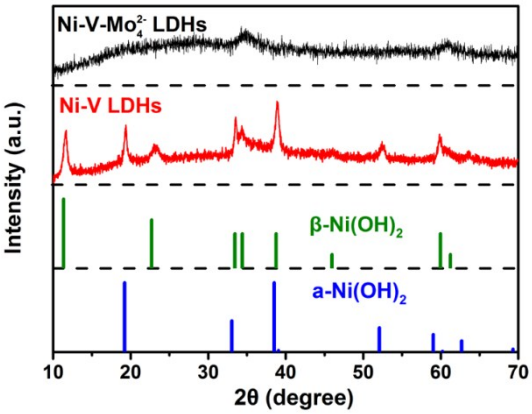

Fig. S4 XRD patterns of Ni-V-MoO_4^{2-} LDHs and Ni-V LDHs.

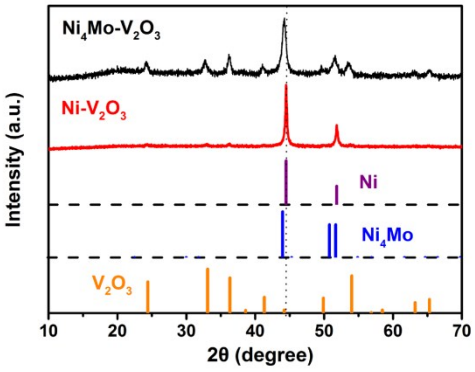

Fig. S5 XRD patterns of Ni-V_2O_3 and Ni_4Mo-V_2O_3.

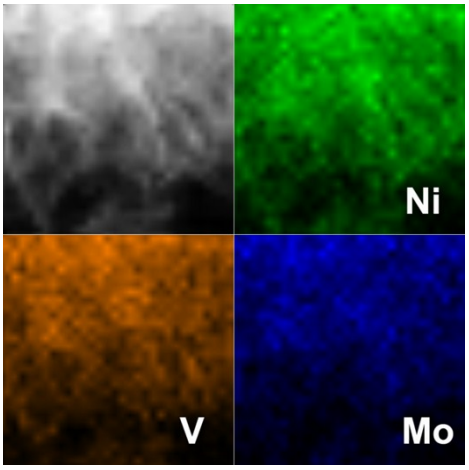

Fig. S6 Scanning transmission electron microscopy (STEM) image and EDS elemental mapping of Ni, V, Mo elements in Ni_4Mo-V_2O_3.

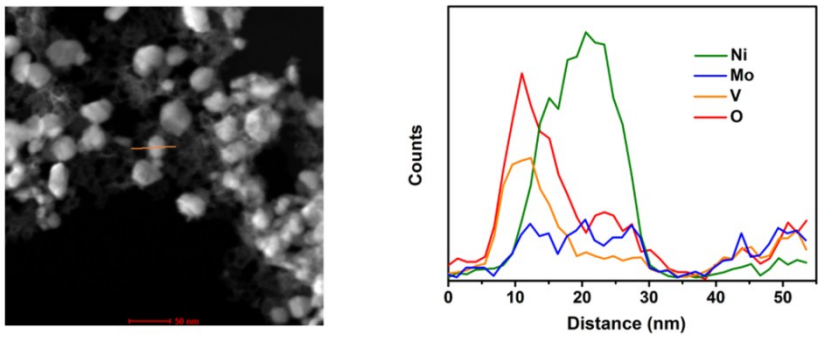

Fig. S7 The line-scan profiles of Ni_4Mo-V_2O_3.

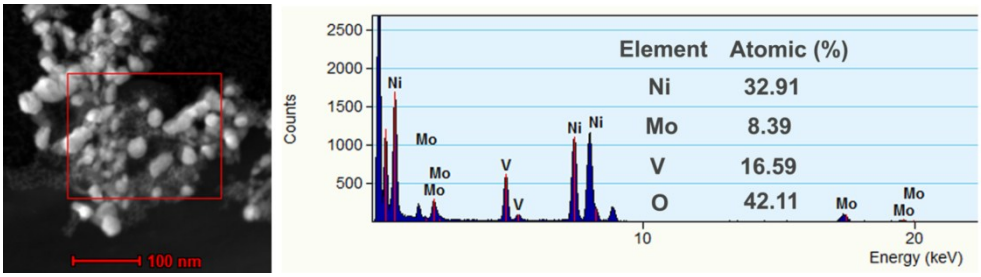

Fig. S8 TEM–EDS data of Ni_4Mo-V_2O_3.

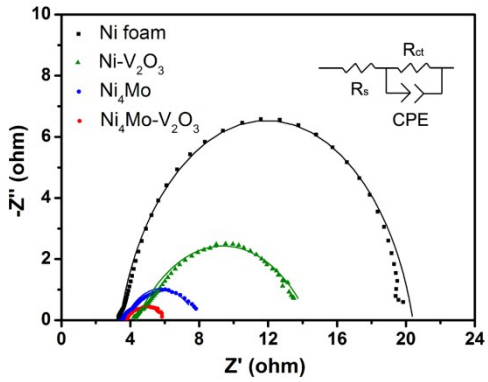

Fig. S9 Nyquist plots of various electrodes from EIS measurements performed at overpotential of 100 mV.

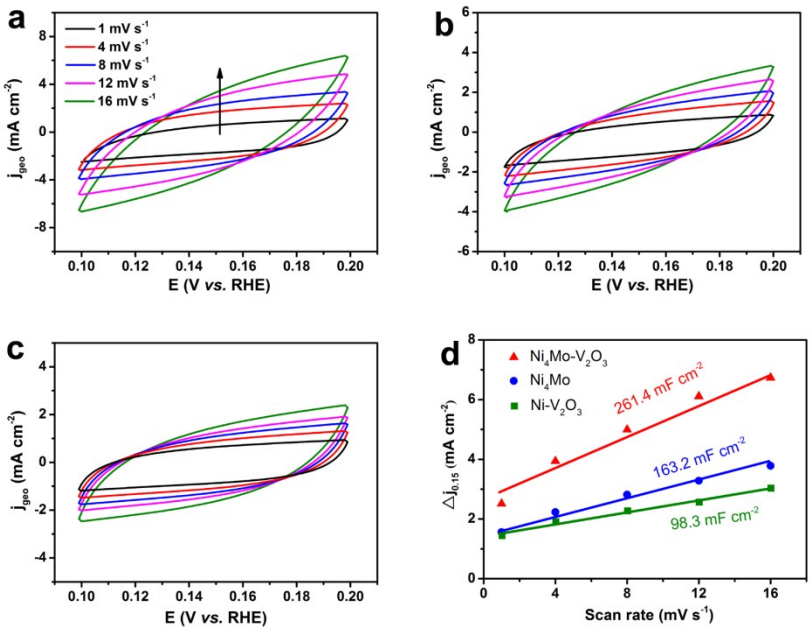

Fig. S10 Electrochemical capacitance measurements for various electrodes. CV were taken in a potential range (0.1 ~ 0.2 V vs. RHE) without Faradic processes for (a) Ni_4Mo-V_2O_3, (b) Ni_4Mo, and (c) Ni-V_2O_3. (d) Plot of the capacitive current determined at 0.15 V as a function of scan rate for Ni_4Mo-V_2O_3, Ni_4Mo, and Ni-V_2O_3.

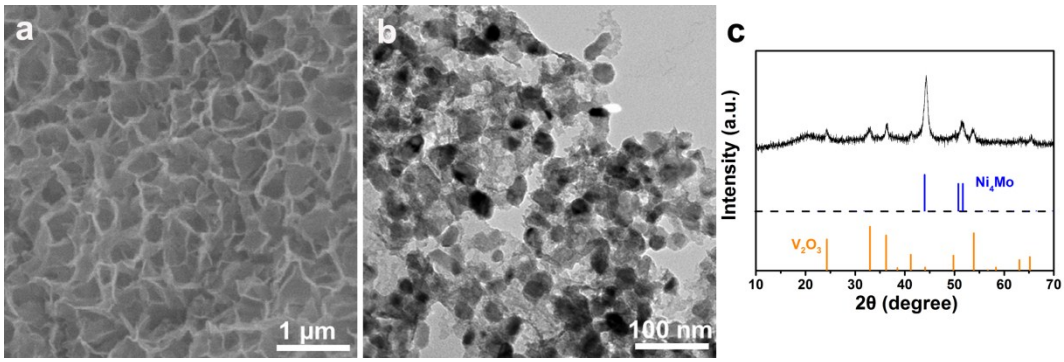

Fig. S11 (a) SEM, (b) TEM, and (c) XRD of Ni_4Mo-V_2O_3/NF after stability test.

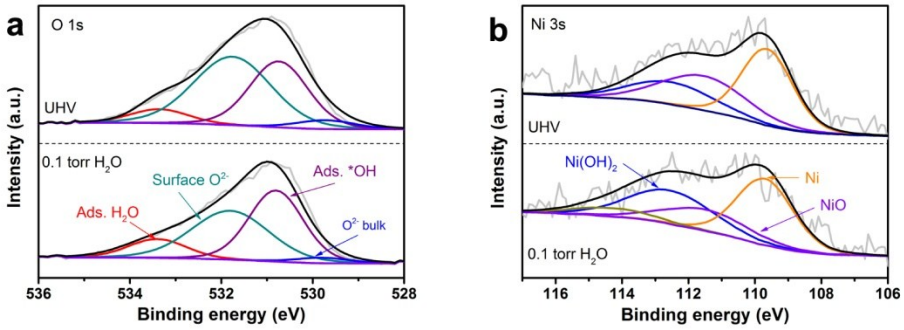

Fig. S12 Near-ambient pressure XPS experiments of water adsorption on Ni-V_2O_3.

Table S1. Comparison of HER performance on different catalysts in neutral media.

Electrocatalysts	η_{10} (mV)	Tafel slope (mV dec^{-1})	Mass Loading (mg cm^{-2})	Ref.
Ni_4Mo-V_2O_3/NF	39.3	65.7	1.7	This work
$NiCo_2P_x$/CF	63.3	63	5.9	Adv. Mater. 2017, 29, 1605502
CrO_x/Cu–Ni	48	64	0.1	Nat. Energy 2018, 4, 107
$Ni_{0.33}Co_{0.67}S_2$	72	67.8	0.3	Adv. Energy Mater. 2015, 5, 1402031
Defective-NiFe LDH	87	46.3	~3	ACS Energy Lett. 2019, 4, 1412
Co-HNP/CC	87	41.7	1	Angew. Chem. Int. Ed. 2016, 55,6725
MoP/CNTs	102	115	0.5	Adv. Funct. Mater. 2018, 1706523
CoP nanorod array	106	93	0.92	J. Am. Chem. Soc. 2014, 136, 7587
FeP nanoparticles	120	70	4.1	ACS Appl. Mater. Interfaces 2014, 6, 20579
CoP/Ti	149	58	2	Chem. Mater. 2014, 26, 4326
Amorphous Co-S film	160	93	—	J. Mater. Chem. A 2014, 2, 13795
CoS/FTO	170	93	—	J. Am. Chem. Soc. 2013, 135, 17699
Ni_3S_2/NF	170	—	1.6	J. Am. Chem. Soc. 2015, 137, 14023
WP nanorod array	200	125	2	ACS Appl. Mater. Interfaces 2014, 6, 21874
FeP nanorod array	202	71	1.5	ACS Catal. 2014, 4, 4065
WP_2	244	92	0.5	ACS Catal. 2014, 5, 145
CoN_x/C	247	—	2	Nat. Commun. 2015, 6, 7992
NiS_2 NA/CC	243	—	4.1	Electrochim Acta. 2015, 153, 508

Table S2. Chemical state of O in Ni_4Mo, Ni-V_2O_3, and Ni_4Mo-V_2O_3 under UHV and water pressure.

Catalyst	Pressure	Chemical state	Binding Energy (eV)	Atomic percentage (%)
Ni_4Mo-V_2O_3	UHV	O^{2-} bulk	529.7	3.9
		Ads. ·OH	530.7	43.8
		Surface O^{2-}	531.8	39.8
		Ads. H_2O	533.4	12.5
	0.1 torr H_2O	O^{2-} bulk	529.7	3.1
		Ads. ·OH	530.7	52.3
		Surface O^{2-}	531.8	24.8
		Ads. H_2O	533.4	19.8
Ni_4Mo	UHV	O^{2-} bulk	529.7	4.0
		Ads. ·OH	530.7	40.5
		Surface O^{2-}	531.8	46.2
		Ads. H_2O	533.4	9.2
	0.1 torr H_2O	O^{2-} bulk	529.7	3.4
		Ads. ·OH	530.7	45.9
		Surface O^{2-}	531.8	36.6
		Ads. H_2O	533.4	14.1
Ni-V_2O_3	UHV	O^{2-} bulk	529.7	4.9
		Ads. ·OH	530.7	36.7
		Surface O^{2-}	531.8	50.7
		Ads. H_2O	533.4	7.7
	0.1 torr H_2O	O^{2-} bulk	529.7	3.3
		Ads. ·OH	530.7	42.7
		Surface O^{2-}	531.8	41.9
		Ads. H_2O	533.4	12.2

Table S3. Chemical state of Ni in Ni_4Mo, Ni-V_2O_3, and Ni_4Mo-V_2O_3 under UHV and water pressure.

Catalyst	Pressure	Chemical state	Binding Energy (eV)	Atomic percentage (%)
Ni_4Mo-V_2O_3	UHV	Ni	109.7	43.9
		NiO	111.5	16.0
		$Ni(OH)_2$	112.5	40.1
	0.1 torr H_2O	Ni	109.7	23.5
		NiO	111.5	17.3
		$Ni(OH)_2$	112.5	53.6
		Ni^{3+}	114.3	5.6
Ni_4Mo	UHV	Ni	109.7	45.7
		NiO	111.5	24.9
		$Ni(OH)_2$	112.5	29.4
	0.1 torr H_2O	Ni	109.7	39.5
		NiO	111.5	16.6
		$Ni(OH)_2$	112.5	36.4
		Ni^{3+}	114.3	7.4
Ni-V_2O_3	UHV	Ni	109.7	44.7
		NiO	111.5	33.5
		$Ni(OH)_2$	112.5	21.8
	0.1 torr H_2O	Ni	109.7	41.3
		NiO	111.5	19.9
		$Ni(OH)_2$	112.5	31.2
		Ni^{3+}	114.3	7.6

Table S4. Adsorption energy of H_2O, H, and OH on the catalysts in terms of Gibbs free energy (G, eV); the energy barriers (△G, eV) of H_2O dissociation step (Volmer step, fifth column) and H* combines to form molecular hydrogen (Tafel step, sixth column) on different catalyst models.

Catalysts	**G (H_2O*)**	**G (OH*-H*)**	**G (H*)**	**ΔG (H_2O)**	**ΔG (1/2H_2)**
Ni_4Mo	-0.41	-0.36	-0.49	0.65	0.49
Ni_4Mo-V_2O_3	-0.51	-1.06	-0.42	0.42	0.42